Cell

Polarization of the Endoplasmic Reticulum by ER-Septin Tethering

Jesse T. Chao,[1] Andrew K.O. Wong,[1] Shabnam Tavassoli,[1] Barry P. Young,[1] Adam Chruscicki,[2] Nancy N. Fang,[2,3] LeAnn J. Howe,[2] Thibault Mayor,[2,3] Leonard J. Foster,[2,3] and Christopher J.R. Loewen[1,*]
[1]Department of Cellular and Physiological Sciences
[2]Department of Biochemistry and Molecular Biology
Life Sciences Institute, University of British Columbia, 2350 Health Sciences Mall, Vancouver BC V6T 1Z3, Canada
[3]Centre for High-Throughput Biology, University of British Columbia, 2125 East Mall, Vancouver BC V6T 1Z4, Canada
*Correspondence: cloewen@mail.ubc.ca
http://dx.doi.org/10.1016/j.cell.2014.06.033

SUMMARY

Polarization of the plasma membrane (PM) into domains is an important mechanism to compartmentalize cellular activities and to establish cell polarity. Polarization requires formation of diffusion barriers that prevent mixing of proteins between domains. Recent studies have uncovered that the endoplasmic reticulum (ER) of budding yeast and neurons is polarized by diffusion barriers, which in neurons controls glutamate signaling in dendritic spines. The molecular identity of these barriers is currently unknown. Here, we show that a direct interaction between the ER protein Scs2 and the septin Shs1 creates the ER diffusion barrier in yeast. Barrier formation requires Epo1, a novel ER-associated subunit of the polarisome that interacts with Scs2 and Shs1. ER-septin tethering polarizes the ER into separate mother and bud domains, one function of which is to position the spindle in the mother until M phase by confining the spindle capture protein Num1 to the mother ER.

INTRODUCTION

Establishment of cell polarity is a fundamental aspect of biology that enables cells to spatially segregate their functions and to divide. Cell polarization is achieved through cytoskeleton-based directional transport of cargo to polarized domains and through the establishment of diffusion barriers that compartmentalize such domains. Similarly to mammalian cells, yeast establish polarity using the highly conserved Ras and Rho-like family of GTPases (for review, see Pruyne et al., 2004). Once a bud site is selected, Cdc42 recruits a yeast-specific polarity complex called the polarisome, comprising Pea2, Spa2, Bud6, and the formin Bni1, which nucleates actin cables in the bud (Evangelista et al., 1997). Myosin motor proteins mediate directional transport of exocytic vesicles on these cables resulting in polarized growth of the bud. During budding, Cdc42 also initiates the formation of a physical diffusion barrier at the neck, comprising septins, which compartmentalizes the bud plasma membrane (PM) from the mother (Dobbelaere and Barral, 2004). Septins belong to a conserved family of large GTPases that assemble into filaments and form continuous PM-associated cytoskeletal structures that physically restrict lateral diffusion of PM proteins (for review, see Caudron and Barral, 2009).

Like the PM, the endoplasmic reticulum (ER) is a single continuous membrane system that is compartmentalized into distinct domains. In yeast, diffusion of integral ER proteins is restricted between the ER in the mother and the ER in the bud, implying a physical diffusion barrier exists between these domains (Luedeke et al., 2005). This barrier is dependent on the septin Shs1 and on two polarisome components, Bud6 and Pea2, and has been proposed to involve direct interactions between septins and the ER that traverses the neck (Luedeke et al., 2005). At least five mRNAs encoding verified ER proteins are polarized to the yeast bud (Shepard et al., 2003), suggesting an important function of the barrier might be to compartmentalize synthesis of ER proteins in the bud, hence, polarizing the ER. We previously identified a role for the conserved ER protein Scs2 in the capture of ER tubules at sites of polarized growth and formation of PM-associated ER (pmaER) in yeast (Loewen et al., 2007). Here, we have uncovered the molecular composition of the ER diffusion barrier in yeast by identifying proteins that interacted with Scs2 at polarized sites.

RESULTS

Epo1 Localizes Scs2 to Sites of Polarized Growth

We previously found that a soluble version of Scs2 lacking the C-terminal transmembrane domain and tagged with GFP (Scs2ΔTM-GFP) localized to sites of polarized growth (Loewen et al., 2007). Now, we identified proteins responsible for polarizing Scs2ΔTM using a quantitative proteomics approach (Chao et al., 2009) (Figure 1A). One protein identified encoded by the ORF *YMR124W* (Figure 1B; Table S1 available online), localized to sites of polarized growth including the incipient bud site in G1, the tips of small and medium buds in S and G2, and the septum during cytokinesis (Figure 1C). These localizations overlapped with many of the localizations of Scs2ΔTM-GFP (Figure 1D). Ymr124w was an excellent candidate for polarizing Scs2 and we named it Epo1 for ER polarization.

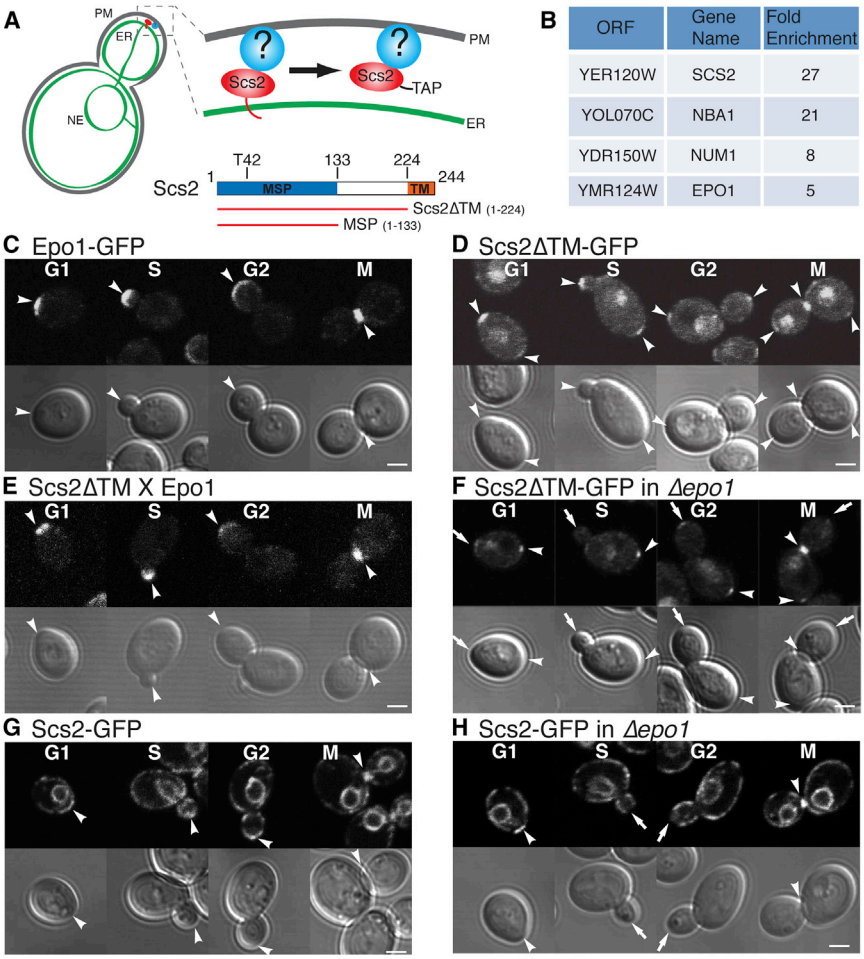

ORF	Gene Name	Fold Enrichment
YER120W	SCS2	27
YOL070C	NBA1	21
YDR150W	NUM1	8
YMR124W	EPO1	5

Figure 1. Epo1 Captures ER Tubules in the Bud

(A) Scs2 interacts with an unknown polarized protein at the bud tip. ER, endoplasmic reticulum; PM, plasma membrane; NE, nuclear envelope.

(B) Scs2ΔTM binding partners having polarized localizations identified by SILAC mass spectrometry. See also Table S1.

(C) Epo1-GFP localization in cells staged throughout the cell cycle. Arrowheads indicate sites of polarized growth.

(D and F) Scs2ΔTM-GFP localization in wild-type (D) and *Δepo1* (F). Arrowheads indicate PM-associated localizations; arrows indicate altered localizations in the mutant.

(E) PCA between Scs2ΔTM and Epo1. Arrowheads indicate sites of interaction.

(G and H) Scs2-GFP localization in wild-type (G) and *Δepo1* (H). Arrowheads indicate regions of the ER enriched for Scs2-GFP; arrows indicate altered localizations in the mutant. All scale bars represent 2 μm. WT, wild-type.

See also Figure S1.

To characterize the Epo1-Scs2 interaction, we employed the Venus protein-fragment complementation assay (PCA) (Michnick et al., 2007). Scs2ΔTM interacted with Epo1 by PCA at sites of polarized growth that overlapped with the localization of Epo1-GFP (Figure 1E). Epo1 did not interact with another abundant type I ER protein Pho88 (Figure S1A). The Epo1 binding site in Scs2 mapped to a conserved region of its MSP domain known to bind the FFAT motif (two phenylalanines in an acidic tract), which is present in multiple protein families with ER-related functions (Figures S1B–S1E) (Loewen et al., 2003). Targeting of Scs2ΔTM-GFP to the tips of small and medium buds was dramatically reduced in *Δepo1* cells (Figure 1F). Quantification of Scs2ΔTM-GFP showed significantly reduced localization to the G1 incipient bud site and targeting was virtually abolished at the tips of small buds (Figures S1F and S1G). Targeting to large G2 buds was also reduced (Figure S1H), but targeting in M phase was not significantly affected (Figure S1I).

Epo1 Attaches ER to the Bud Cortex

Now, we localized full-length Scs2-GFP that appeared functional (Figure S1J), in wild-type and *Δepo1* cells. Scs2-GFP localized throughout the ER and was enriched at sites of polarized growth (Figure 1G) similar to Scs2ΔTM-GFP. Scs2-GFP was lost from the distal cortex of the bud during S and G2 phases in *Δepo1* cells consistent with Epo1 localizing Scs2ΔTM-GFP to these sites (Figures 1H and S1K). Because this also suggested a defect in pmaER in the mutant, we compared ER in small buds of *Δepo1* and *Δscs2* cells using Pho88 tagged with GFP. Both the *Δepo1* and *Δscs2* mutants showed a clear lack of pmaER at the distal bud cortex (Figure S1L). Thus, the interaction between Epo1 and Scs2 was required for capture of ER tubules at the distal bud cortex.

Epo1 Interacts with the Polarisome

Epo1 is a soluble 944 amino acid protein with a predicted coiled-coil domain (CCD) at its C terminus (Figures 2A and S2A). A high-throughput yeast 2-hybrid study of yeast CCDs (Newman et al., 2000) identified an interaction between the CCD of Epo1 and the CCD of Pea2 (Figure 2A), suggesting that Epo1 might interact with the polarisome. Our proteomic analysis using Epo1-TAP identified that Epo1 interacted with multiple proteins with roles in cell polarity including Pea2 (Table S2). We were able to pull-down MBP-tagged Pea2 CCD using GST-tagged Epo1 CCD, whereas neither protein interacted with control proteins (Figure 2B). Using PCA full-length Epo1 interacted with Pea2 at sites of polarized growth that corresponded to the localizations of Pea2-GFP (Figures 2C and 2D). The CCDs of Epo1 and Pea2 also interacted in vivo by PCA (Figures 2E and 2F). Finally, deletion of the Epo1 CCD prevented its interaction with Pea2 by PCA (Figure 2G). Together, these data indicated Epo1 and Pea2 interacted via their CCDs.

The Pea2-Epo1 interaction suggested that Pea2 might localize Epo1. Consistent with this deletion of *PEA2* resulted in

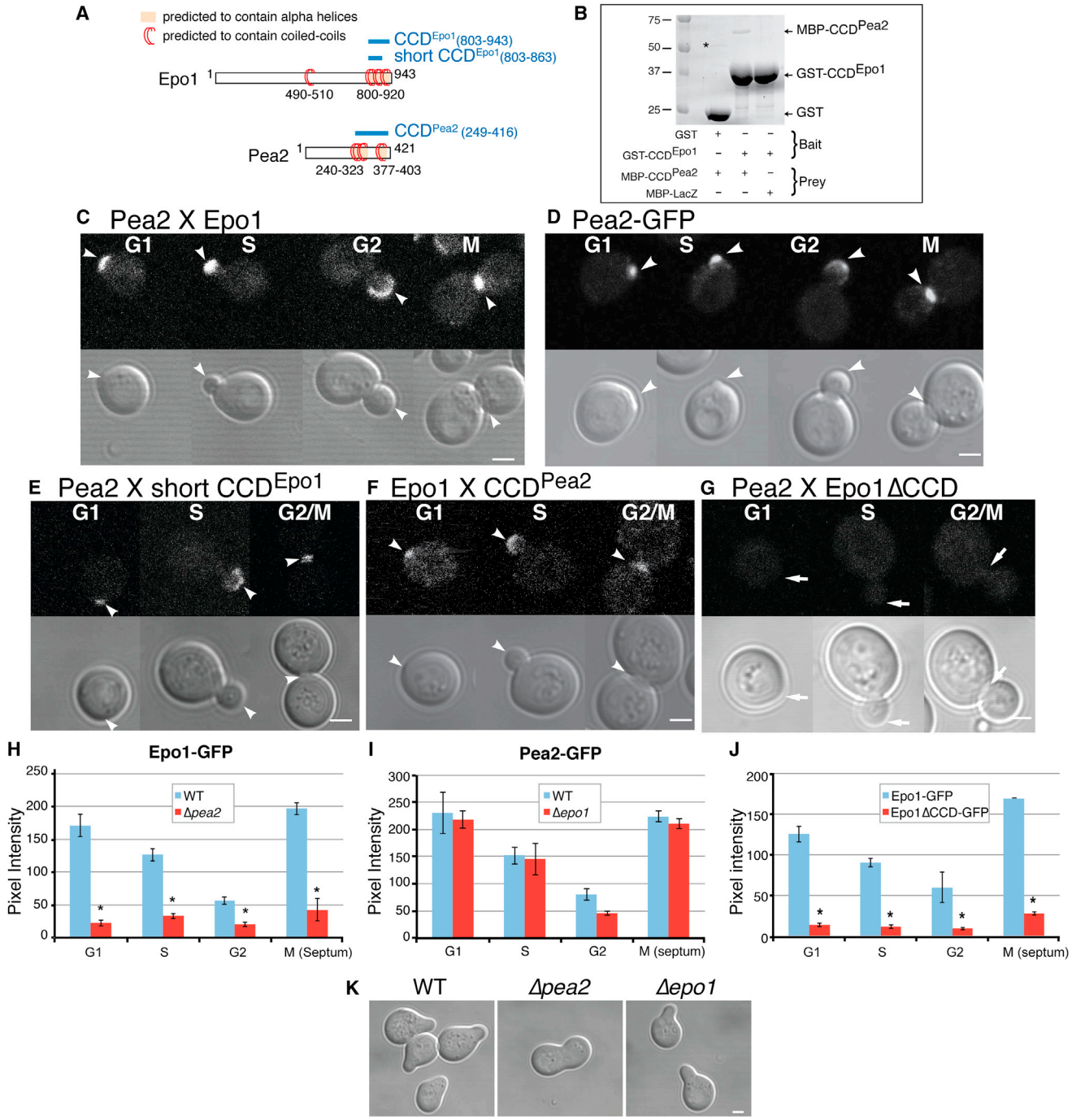

Figure 2. Epo1 Is a Subunit of the Polarisome

(A) Schematic of domain organizations of Epo1 and Pea2. Regions in Epo1 and Pea2 identified to bind each other by yeast two hybrid analysis are labeled (CCD^{Pea2}; short CCD^{Epo1}) (Newman et al., 2000). A longer version of the Epo1 coiled-coil domain (CCD^{Epo1}) used for binding studies in (B) is also shown.

(B) Purified recombinant GST-fusion proteins were immobilized on glutathione beads and incubated with purified recombinant MBP-fusion proteins. Bound fractions were analyzed by SDS-PAGE and Coomassie staining. Asterisk, minor contaminant band present in purified GST fraction alone.

(C) PCA between Pea2 and Epo1.

(D) Pea2-GFP localization.

(E and F) PCA between Pea2 and CCD^{Epo1} (E) and Epo1 and CCD^{Pea2} (F). CCD^{Epo1} and CCD^{Pea2} were expressed from plasmids.

(G) PCA between Pea2 and Epo1ΔCCD. Arrows indicate altered localizations compared to full-length Epo1.

(H) Quantification of Epo1-GFP at polarized sites in wild-type (WT) and *Δpea2* cells. A minimum of 25 cells were measured per localization. Asterisks, $p < 0.05$ versus WT.

(legend continued on next page)

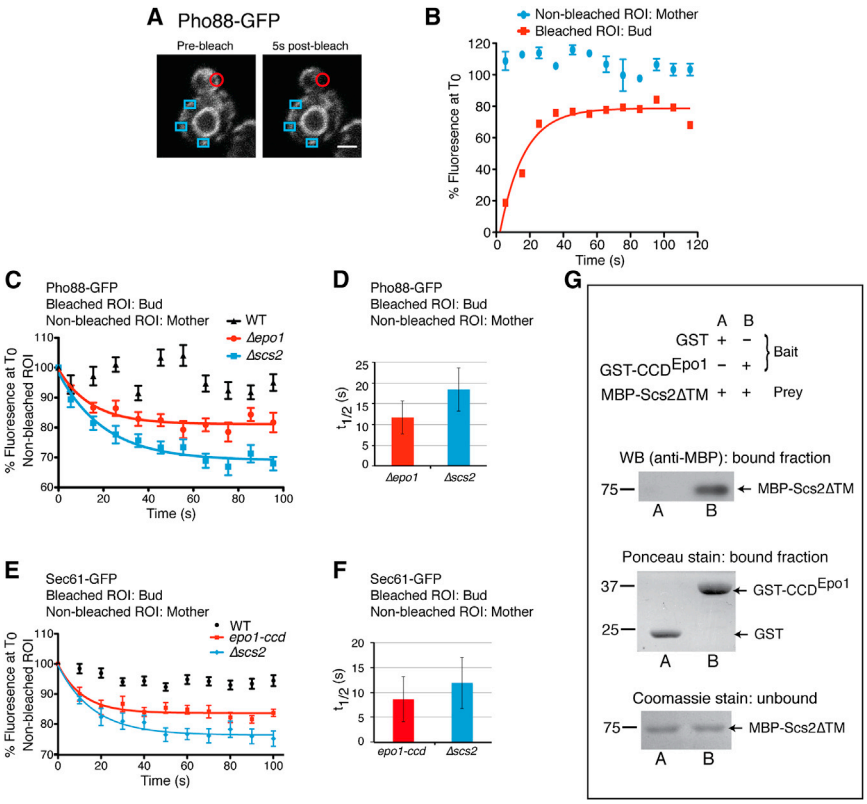

Figure 3. Epo1 and Scs2 Are Required for the ER Diffusion Barrier

(A) Confocal images of a wild-type cell expressing Pho88-GFP before and 5 s after photobleaching a region of pmaER in the bud (red circle). Changes in fluorescence were monitored within the bleached ROI and within three nonbleached ROIs in the mother (blue boxes). Scale bar represents 2 μm.

(B) For the cell in (A), changes in fluorescence within the bleached and nonbleached ROIs were plotted over time as % fluorescence relative to prebleach (T_0). Fluorescence recovery within the bleached ROI was fitted to a single exponential function.

(C) Similar to (A), but for multiple cells of wild-type (WT), *Δepo1* and *Δscs2* mutants (minimum of five cells per strain).

(D) Rates of fluorescence loss were calculated for *Δepo1* and *Δscs2* cells photobleached in (C) and plotted as $t_{1/2}$ values.

(E and F) As in (C and D), except with cells expressing Sec61-GFP.

(G) Purified recombinant GST-fusion proteins were immobilized on glutathione beads and incubated with purified recombinant MBP-fusion proteins. Bound fractions were analyzed by western blotting (WB) and Ponceau S stain. Unbound fractions were analyzed by SDS-PAGE and Coomassie stain. All error bars represent SEM.

See also Figure S3.

quantitative loss of Epo1-GFP from sites of polarized growth, although some residual localization remained (Figures 2H and S2B). In contrast Epo1 was not required to localize Pea2-GFP (Figure 2I). Deletion of the Epo1 CCD also prevented its polarization (Figures 2J and S2C), indicating interaction of the Epo1 CCD with Pea2 mediated polarization of Epo1. We now tested if Epo1 contributed to the core function of the polarisome in nucleating actin cables by assessing "shmoo" formation. In contrast to *Δpea2* cells, which showed an aberrant "peanut"-shaped shmoo, the *Δepo1* mutant was indistinguishable from wild-type (Figure 2K). Lastly Pea2 did not interact with Scs2 by PCA (Figure S2D) further supporting a specific role for Epo1 in cortical capture of ER tubules.

ER Polarization Requires Epo1 and Scs2

Pea2 was previously identified to be required for formation of the ER diffusion barrier, and we now reasoned that Epo1 and Scs2 might play a role. To test for roles for Epo1 and Scs2, we performed ER photobleaching experiments. We validated the use of Pho88-GFP as a general marker for diffusion of proteins within the ER. We photobleached a small region of the mother pmaER and measured fluorescence recovery within the bleached region (Figures S3A and S3B). Fluorescence recovered quickly within the bleached region with a $t_{1/2}$ of 18 ± 4 s; and Pho88-GFP showed a substantial mobile fraction of ~72% (Figures S3C and S3D). In these same cells, we also measured loss in fluorescence within three nonbleached regions in the mother pmaER (Figure S3A). Upon photobleaching, Pho88-GFP was rapidly lost from these regions with a $t_{1/2}$ of ~10 ± 3 s (Figures S3E and S3F) indicating that a diffusion barrier was not present between regions within the mother ER.

Now, we examined diffusion of Pho88-GFP between mother and bud. We photobleached a region of pmaER in the bud and monitored three nonbleached regions in the mother, initially for a single cell (Figure 3A). Photobleaching of the bud ER did not lead to loss in fluorescence in the mother ER (Figure 3B). Within the bleached region in the bud, fluorescence recovered rapidly (Figure 3B). Together, this indicated a diffusion barrier existed between the bud and mother ER. In *Δepo1* and *Δscs2* cells, we observed a rapid loss in fluorescence in the mother ER upon bleaching the bud ER, whereas wild-type showed no change as before (Figure 3C). We calculated $t_{1/2}$ values of 11 ± 4 s and 18 ± 5 s for *Δepo1* and *Δscs2* cells, respectively (Figure 3D), which were similar to $t_{1/2}$ values for diffusion within bud and mother ER compartments. Diffusion of Pho88-GFP within the mother pmaER in *Δepo1* and *Δscs2* cells was similar to wild-type (Figures S3B–S3F) indicating the ER membrane

(I) As in (H), but with Pea2-GFP in WT and *Δepo1* cells. No significant differences were observed.

(J) As in (H), but with Epo1-GFP and Epo1ΔCCD-GFP.

(K) Alpha factor treatment of WT, *Δpea2* and *Δepo1* cells. All scale bars represent 2 μm. All error bars represent SEM.

See also Figure S2.

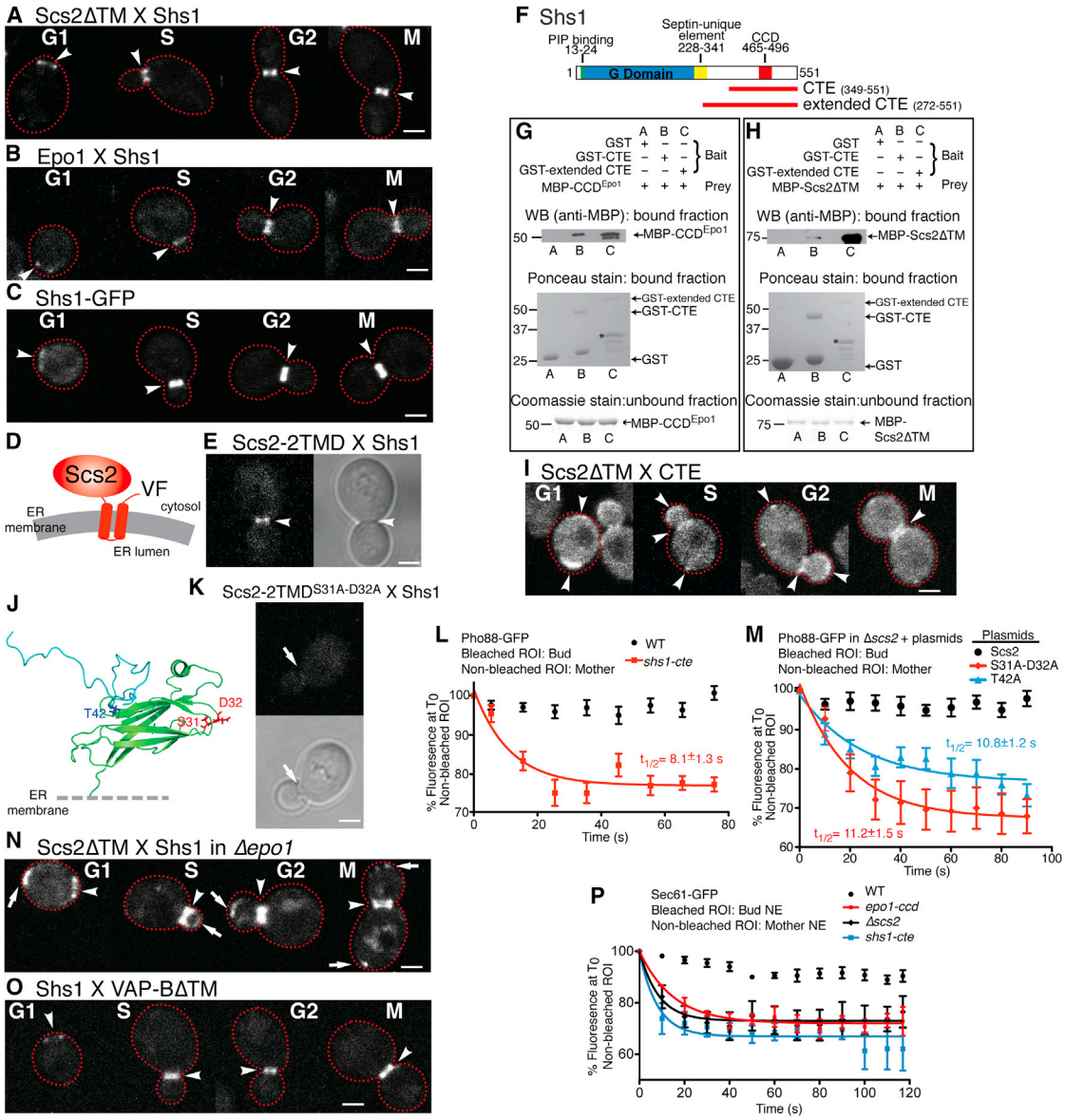

Figure 4. Shs1 Interacts with Epo1 and Scs2 Creating the ER Diffusion Barrier

(A and B) PCA with the indicated proteins. Arrowheads indicate sites of interaction. Red dotted line identifies the perimeter of each cell.

(C) Shs1-GFP localization.

(D) Diagram depicting the engineering of Scs2-2TMD, which replaces the single C-terminal transmembrane domain of Scs2 with the two transmembrane domains of Sac1 fused to one half of Venus YFP (VF).

(E) PCA between Scs2-2TMD expressed from a plasmid and Shs1.

(F) Schematic of domain organizations of Shs1 (Versele et al., 2004). Regions in Shs1 used in this study are shown underneath the protein. PIP, phosphoinositide; G domain, GTP-binding; CCD, coiled-coil domain; CTE, C-terminal extension.

(G and H) Binding of the Epo1 CCD (G) and Scs2ΔTM (H) to the Shs1 CTE in vitro. Binding of purified recombinant bait and prey fusion proteins was performed as in Figure 3G. Asterisks, break down products of GST-fusion proteins.

(I) PCA between Scs2ΔTM and the CTE of Shs1 expressed from a plasmid. Arrowheads indicate strong PCA signals.

(J) Ribbon diagram of the NMR structure of human VAP-A (green) in complex with the FFAT motif of human OSBP (blue) generated using PyMOL (Furuita et al., 2010). The location of the T42A mutation that disrupts FFAT motif binding as well as the newly identified S31 and D32 residues involved in Shs1 binding are highlighted (the equivalent residues in VAP-A are shown with Scs2 numbering).

(K) PCA between Scs2-2TMD-S31A-D32A expressed from a plasmid and Shs1. The arrow indicates the location of the septin ring.

(L) Photobleaching analysis, similar to Figure 3C, except for wild-type (WT) and *shs1-cte* cells (minimum of five cells each; $t_{1/2}$ value is given on graph).

(M) Photobleaching analysis, similar to Figure 3C, except for Δ*scs2* expressing wild-type Scs2 or point mutants of Scs2 (S31A-D32A or T42A) from plasmids (seven cells each; $t_{1/2}$ values are given on graph).

(legend continued on next page)

environment was unaltered in the mutants. Thus, Epo1 and Scs2 were required for the ER diffusion barrier.

We now investigated whether the Epo1 CCD was required for the diffusion barrier. Similar photobleaching experiments using Sec61-GFP, which diffused rapidly within the pmaER in the bud and was highly mobile (Figures S3G–S3J), revealed that the barrier was compromised in the *epo1-ccd* mutant (Figures 3E and 3F). Given the importance of the Epo1 CCD for the diffusion barrier, we tested whether this region also bound to Scs2. Purified recombinant Scs2 MSP domain tagged with MBP bound to GST-Epo1 CCD, but not to GST alone (Figure 3G). Using PCA, deletion of the Epo1 CCD prevented interaction with Scs2 in vivo, consistent with Scs2 binding the CCD (Figure S3K).

Epo1, Scs2, and Shs1 Form an ER-Septin Tether at the Bud Neck

The role for the septin Shs1 in creating the ER diffusion barrier suggested it might physically interact with Epo1 and Scs2 to form an ER-septin tether. Using PCA, both Epo1 and Scs2 interacted with Shs1 as a pair of punctae at the incipient bud site in G1, at the bud neck throughout the cell cycle and at the septum during cytokinesis (Figures 4A and 4B). These localizations closely corresponded to the localization of Shs1-GFP (Figure 4C) and were indicative of the septin complex. Pea2 did not interact with Shs1 by PCA (Figure S4A). We also verified these interactions by PCA with the dehydrofolate reductase (DHFR) enzyme, which is noninteraction-trapping (Figure S4B) (Tarassov et al., 2008). Scs2ΔTM-GFP copurified with Shs1-TAP, but not in the control, indicating the presence of a stable interaction between these proteins in yeast (Figure S4C). Shs1-GFP also copurified with Epo1-TAP from yeast (Figure S4D). These results suggested that Scs2 and Epo1 interacted with Shs1 throughout the cell cycle; at the incipient bud site in G1, at the bud neck in S, G2, and M phase and at the septum during cytokinesis.

To directly visualize tethering in vivo between the ER and septins we engineered a fusion protein, Scs2-2TMD, that contained the MSP domain of Scs2 and the two transmembrane domains of the ER protein Sac1, followed by the Venus PCA fragment (Figure 4D) that should place both the MSP domain and the PCA fragment on the cytoplasmic face of the ER membrane. A GFP-tagged version localized throughout the ER and the PCA version interacted with a canonical FFAT motif sequence on the ER (Figure S4E). Shs1 interacted with Scs2-2TMD by PCA discretely at the bud neck, thus demonstrating the physical tethering of ER to septins within the neck (Figure 4E).

Shs1 has, in addition to the GTPase domain present in all septins, a C-terminal extension (CTE) that contains a CCD (Figure 4F) (Garcia et al., 2011), raising the possibility that this region interacted with the Epo1 CCD. Purified recombinant GST-tagged CTE interacted specifically with MBP-Epo1 CCD (Figure 4G). We detected increased binding to a longer version of the CTE that was extended 77 amino acids N-terminally (Figures 4F and 4G). By PCA, the Epo1 CCD interacted with full-length Shs1 in vivo, as did the CTE with full-length Epo1 (Figures S4F and S4G). Deletion of the CTE prevented interaction between Shs1 and Epo1, even though Shs1ΔCTE-GFP localized normally to the neck (Figures S4H and S4I). Deletion of the Epo1 CCD also prevented binding to Shs1 (Figure S4J).

Now, we reconstituted binding in vitro between Scs2 and Shs1. Purified recombinant GST-tagged Shs1 CTE and the extended CTE both interacted specifically with MBP-Scs2 (Figure 4H). The CTE interacted with Scs2ΔTM by PCA at sites of polarized growth as well as the bud neck (Figure 4I). Deletion of the CTE prevented interaction between Shs1 and Scs2 at the bud neck (Figure S5A). The Scs2 MSP domain alone interacted with Shs1 (Figure S5B); however, the T42A mutation did not disrupt binding, indicating that CTE binding was distinct from Epo1 and FFAT motif binding (Figure S5C). Therefore, we conducted a structure-based directed mutagenesis screen of the Scs2 MSP domain using the Venus PCA between Scs2-2TMD and Shs1. Mutation of two consecutive residues, S31 and D32, in a solvent accessible loop region of Scs2 (Figure 4J; Table S3), prevented interaction of Scs2-2TMD with Shs1 at the bud neck (Figure 4K). The S31A-D32A mutant, however, was capable of binding to Epo1 by PCA and rescued the pmaER defect of *Δscs2* cells (Figures S5D and S5E). Mutation of this loop also did not interfere with the function of Scs2 in binding and regulation of the FFAT motif-containing protein, Opi1, in vivo (Figure S5F). Together, these data supported that Scs2 interacted with the CTE of Shs1 via an accessible loop located on the opposite face of the MSP domain to its FFAT motif and Epo1 binding sites. Finally, localization of Scs2ΔTM-GFP to the septum in *shs1-cte* cells was dramatically reduced (Figures S5G and S5H), indicating that binding to the CTE was required to recruit Scs2 to the septin ring in vivo.

ER-Septin Tethering Creates the ER Diffusion Barrier

Interaction of Scs2 and Epo1 with Shs1 suggested that ER-septin tethering was responsible for the ER diffusion barrier, and we now focused on a role for the Shs1 CTE. The Shs1 CTE is required for septin ring formation in vitro, but not for incorporation of Shs1 into octamers (Garcia et al., 2011) and its role in vivo is unknown. Loss of Shs1 results in minor defects in septin organization and aberrant cytokinesis, which causes growth arrest under cold stress (Iwase et al., 2007). The CTE was not required for Shs1 incorporation into septin filaments in vivo (Figure S4I); and deletion of the CTE did not result in sensitivity to growth (Figure S5I) or budding defects (Figure S4I), suggesting the CTE was dispensable for cytokinesis. However, loss of the CTE in the *shs1-cte* mutant clearly compromised the ER diffusion barrier (Figure 4L). The $t_{1/2}$ value of 8 ± 1 s indicated that Pho88-GFP diffused between bud and mother in the *shs1-cte* mutant at the

(N) PCA between Scs2ΔTM and Shs1 in Δ*epo1* cells. Arrowheads indicate sites of interaction at septin rings. Arrows indicate mislocalized interactions in the *Δepo1* mutant.

(O) PCA between Shs1 and human VAP-BΔTM expressed from a plasmid.

(P) Photobleaching analysis of the nuclear envelope. A region of the bud nuclear envelope (NE) was bleached and fluorescence values in nonbleached ROIs in the mother NE were measured for the indicated strains expressing Sec61-GFP. All scale bars represent 2 μm. All error bars represent SEM.

See also Figures S4 and S5.

same rate as within the mother in wild-type ($t_{1/2}$ 9 ± 3 s, Figure S3F). This was not a result of changes in mobility within the ER membrane (Figures S5J–S5L). We also tested if the CTE was required for the PM diffusion barrier by photobleaching a peripheral PM reporter protein, GFP-Lact-C2, which binds phosphatidylserine in the PM and is highly mobile (Figures S5M and S5N) (Spira et al., 2012). In both wild-type and the *shs1-cte* mutant, there was restricted diffusion of GFP-Lact-C2 between the mother and bud indicating that the PM diffusion barrier was intact in *shs1-cte* cells (Figures S5O and S5P).

To determine if the Scs2-Shs1 interaction was responsible for the ER diffusion barrier, we determined if the Scs2 S31A-D32A mutant could generate a diffusion barrier. In contrast to adding wild-type Scs2 on a plasmid back to *Δscs2* cells, which resulted in formation of a barrier, the S31A-D32A mutant failed to produce a diffusion barrier (Figure 4M). We now examined the role for Epo1. The T42A mutant of Scs2, which disrupted binding to Epo1, but not Shs1, also failed to produce a diffusion barrier (Figure 4M), indicating that binding of Scs2 to Epo1 was required. However, deletion of Epo1 did not affect the ability of Scs2 to bind Shs1 purified from yeast (Figure S4C). Deletion of Epo1 resulted in substantial mislocalization of the Scs2-Shs1 PCA to the mother distal pole in G1 and to the bud tip in S, G2, and M phase (compare Figures 4N and 4A), suggesting the role for Epo1 was to maintain a diffusion barrier-competent Scs2-Shs1 interaction at the neck. Finally, because Scs2 is highly conserved, we tested for an interaction between its human homolog, VAP-B, and Shs1 in yeast. VAP-B interacted with Shs1 similarly to Scs2 (Figure 4O), indicating that the ER-septin tether may be conserved in humans.

ER-Septin Tethering Creates the Nuclear Envelope Diffusion Barrier

During mitosis and nuclear migration in yeast, the intact nuclear envelope is pulled through the bud neck into the bud. An ER diffusion barrier has been identified in the nuclear membrane in M phase, which also requires Shs1, implying that a similar mechanism underlies this barrier (Shcheprova et al., 2008). Therefore, we tested for a role for the ER-septin tether in restricting diffusion within the nuclear envelope in M phase cells. Photobleaching analysis with Sec61-GFP revealed that a diffusion barrier indeed existed in the nuclear ER of wild-type cells (Figure 4P). Deletion of the Shs1 CTE, the Epo1 CCD, or Scs2, compromised the diffusion barrier (Figures 4P and S5Q). Thus, the Scs2-Shs1 tether also controlled diffusion of integral proteins within the nuclear membrane during M phase.

Polarization of the Integral ER Protein Ist2 Is Mediated by the ER Diffusion Barrier

Certain mRNAs encoding ER proteins are targeted to the bud (Shepard et al., 2003), indicating they are likely translated in the bud, and implying their protein products may be asymmetrically distributed within the ER. The Ist2 mRNA is polarized to the bud (Takizawa et al., 2000) and encodes a polytopic integral membrane protein that localizes to pmaER (Fischer et al., 2009), although it was initially thought to be integral to the PM (Takizawa et al., 2000). The Ist2 mRNA accumulates in G2/M phase buds and consistently, the Ist2 protein is translated specifically in large buds (Takizawa et al., 2000). Bud synthesized Ist2 does not diffuse back to the mother unless septins are disrupted (Takizawa et al., 2000), suggesting that the ER diffusion barrier might be responsible for polarizing Ist2 within the ER.

We investigated the distribution of Ist2 in wild-type and in ER-septin tethering mutants. In wild-type, GFP-Ist2 localized nonuniformly to the mother cell cortex and was absent from ER tubules and the nuclear ER (Figure 5A). This localization was similar to Tcb3-GFP, an integral ER protein that localizes to pmaER (Figure 5B) (Toulmay and Prinz, 2012). However, GFP-Ist2 was clearly absent from small and medium sized buds (S and G2 phases) and reappeared in M phase buds (Figure 5A). In contrast, Tcb3-GFP was present in both buds and mothers (Figure 5B). Thus, even though pmaER was present in S and G2 phase buds, GFP-Ist2 was restricted to the mother pmaER domain until M phase. In contrast, in the *shs1-cte* mutant, GFP-Ist2 was present in pmaER in S and G2 phase buds (Figure 5C). pmaER appeared normal in the *shs1-cte* mutant (Figure 5D), indicating that in the absence of ER-septin tethering, Ist2 diffused from the mother into the bud. In S phase wild-type cells, the ratio of GFP-Ist2 in mothers versus buds approached 5:1, whereas in the *shs1-cte* mutant it was near 1:1 (Figure 5E). In large budded G2/M phase cells, the ratio was close to 1:1 for both wild-type and mutant (Figure 5E). We observed a similar loss of Ist2 polarization in *Δepo1* and *Δscs2* mutants (Figures 5F and 5G), consistent with the role for ER-septin tethering in polarizing the ER. We also observed lack of pmaER at the tips of S phase buds in these mutants, consistent with the roles for Epo1 and Scs2 in ER tubule capture and pmaER formation.

The ER Diffusion Barrier Functions in S Phase Spindle Positioning

To uncover physiological functions for ER polarization, we interrogated the known global genetic interaction network in yeast, which provides a functional map of the cell (Costanzo et al., 2010). This data set contains over five million unbiased quantitative measurements of synthetic genetic interactions covering over 75% of the yeast genome. We used this data set and performed hierarchical clustering to generate gene clusters having similar genetic interaction profiles in order to identify genes with similar functions. We noticed that *SCS2* was present in a cluster with genes that function in S phase spindle positioning, suggesting a role for ER polarization in this pathway (Figure 6A, "S Phase Cluster"). Genes in the S phase cluster formed aggravating genetic interactions with a gene cluster containing M phase spindle positioning genes (Figure 6A, "M Phase Cluster") as previously observed (Tong et al., 2004). Thus, the presence of *SCS2* within the S phase cluster and its aggravating genetic interactions with genes in the M phase cluster suggested a role for *SCS2* and possibly the ER diffusion barrier in S phase spindle positioning.

To evaluate the role for Scs2 in spindle positioning, we performed our own SGA analysis, which identified aggravating genetic interactions between *SCS2* and many of the genes involved in M phase spindle positioning and nuclear migration (Figure S6A; Tables S4 and S5). We confirmed genetic interactions between *SCS2* and dynein, dynactin, and *NUM1*, and consistent with a role for Scs2 in S phase spindle positioning, these double mutants showed slow growth phenotypes (Figure 6B). Now, we examined

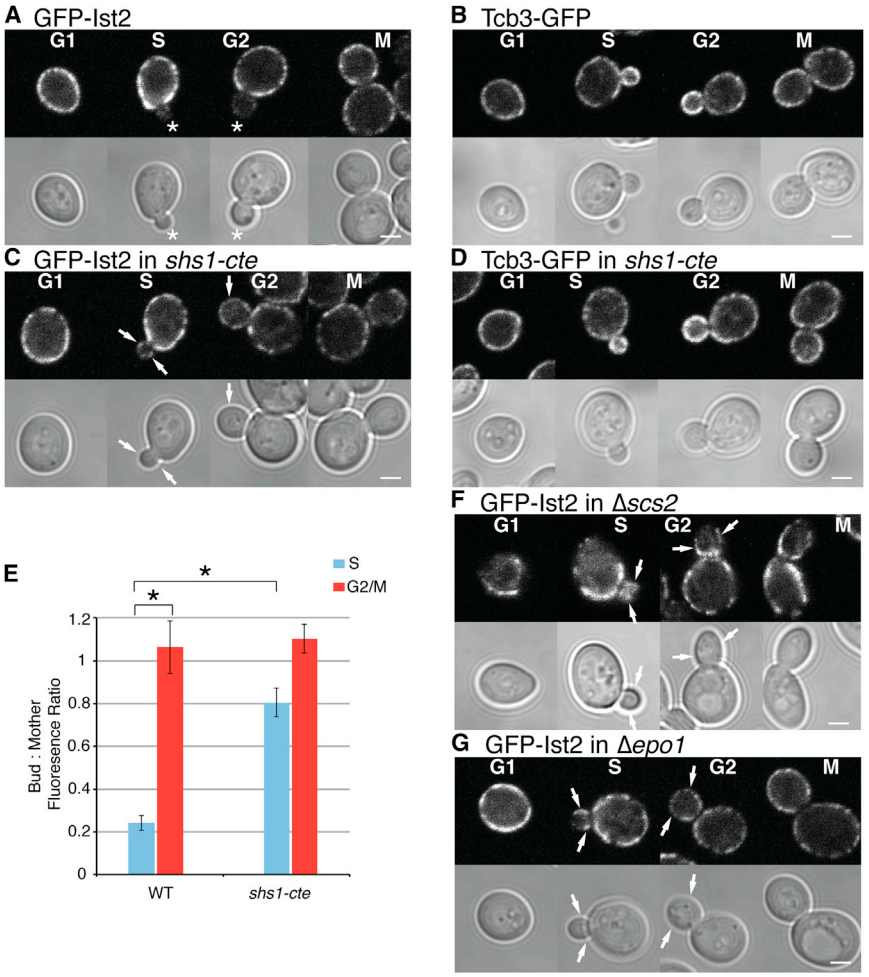

Figure 5. Ist2 Is Polarized within the ER by the ER Diffusion Barrier

(A and C) GFP-Ist2 localization in wild-type (A) and *shs1-cte* (C) cells. Asterisks indicate the absence of localization at the bud cortex. Arrows indicate mislocalization of GFP-Ist2 in the mutants.

(B and D) Tcb3-GFP localization in wild-type (B) and *shs1-cte* (D) cells.

(E) Quantification of the bud to mother fluorescence ratio of GFP-Ist2 in wild-type (WT) and the *shs1-cte* mutant in S and G2/M phase cells. A minimum of 36 cells per category was measured. *$p < 0.0001$.

(F and G) GFP-Ist2 localization in *Δscs2* (F) and *Δepo1* (G) cells. Arrows indicate mislocalization of GFP-Ist2 in the mutants. All scale bars represent 2 μm. All error bars represent SEM.

spindle positioning in wild-type and *Δscs2* cells synchronized in S phase. In wild-type cells, the spindle was predominately positioned in the mother adjacent to the neck (Figures 6C and 6D) (Yeh et al., 1995). In contrast, in *Δscs2* cells the spindle was no longer retained in the mother, but instead migrated into the neck, and in ~13% of cells the spindle mislocalized entirely into the bud clear of the neck. Spindle length was normal in *Δscs2* cells ruling out a role for defective spindle assembly (Figure S6B). Thus, proper S phase spindle positioning relied on Scs2 as indicated by its coclustering with S phase spindle components.

To determine if spindle positioning was related to the diffusion barrier function of Scs2, we examined the ability of Scs2 mutants to rescue spindle mispositioning in *Δscs2* cells. In contrast to adding wild-type Scs2 back on a plasmid, the S31A-D32A mutant failed to restore spindle positioning (Figure 6E). Thus, interaction of Scs2 with Shs1 was required. The T42A mutant also failed to restore spindle positioning. In the *shs1-cte* mutant, the spindle mispositioned entirely into the bud in ~20% of cells and in ~30% of the cells it migrated from the mother into the neck (Figure 6F). Thus, ER-septin tethering functioned to retain the spindle in the mother during S phase. We also tested for genetic interactions between *shs1-cte* cells and mutants in dynein and dynactin, which are critical components of the M phase cluster. We observed slow growth phenotypes for the double mutants over the single-mutant controls in both cases, confirming the presence of aggravating genetic interactions between the *shs1-cte* mutant and the M phase spindle translocation apparatus, similar to loss of *SCS2* (Figures 6G and 6H).

Scs2 Interacts with the Spindle Capture Protein Num1 that Is Required for S Phase Spindle Positioning

We now focused on the mechanism of spindle positioning by the ER diffusion barrier. An important clue came from our proteomics experiment with Scs2ΔTM, which identified an interaction with Num1 (Figure 1B). Num1 is the cortical-localized factor that assembles into patches at the bud tip with dynein and dynactin that form microtubule capture sites, which capture astral microtubules and pull the spindle through the neck into the bud during the process of nuclear migration (Tang et al., 2012). Loss of any of these components results in binucleate mother cells (Farkasovsky and Küntzel, 1995). The cortical localization of Num1 is undefined, and Num1 is curiously absent from S phase buds, until its expression in G2/M phase, when it reappears as a patch at the bud tip (Farkasovsky and Küntzel, 1995). This suggested interaction of Scs2 with Num1 might be responsible for its cortical localization, and that as a peripheral ER protein, Num1 might be restricted from diffusing into S phase buds by the ER diffusion barrier.

First, we characterized the Scs2-Num1 interaction. By coimmunoprecipitation (coIP) GFP-Num1 specifically bound to Scs2ΔTM-TAP in yeast (Figure 7A). Using PCA, full-length Num1 interacted with Scs2-2TMD at the cortex similarly to previously observed localizations of Num1-GFP (Figure S6C; see also Figure 7D) (Heil-Chapdelaine et al., 2000). We noticed an acidic stretch of residues in Num1 that contained

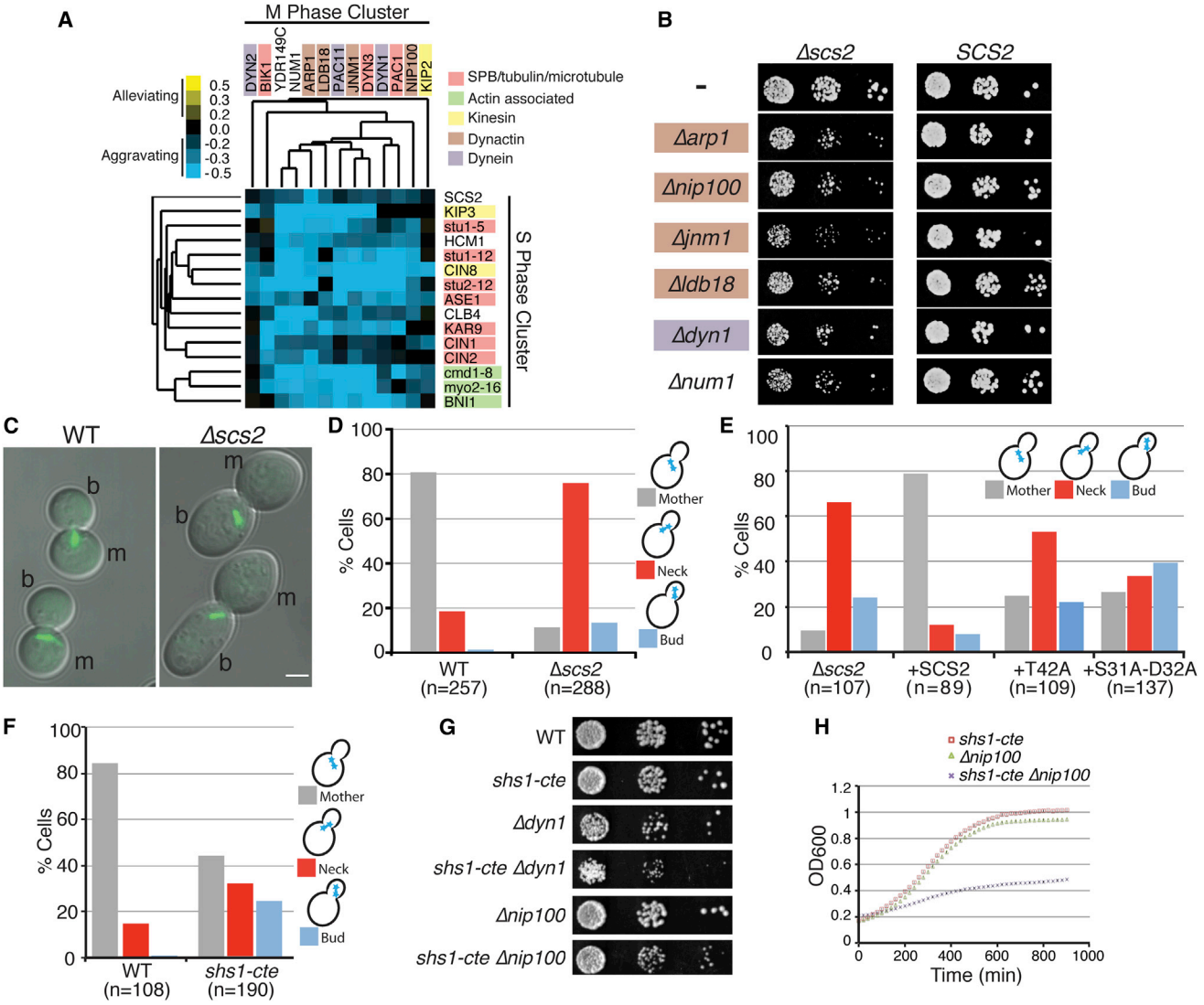

Figure 6. The ER Diffusion Barrier Functions in S Phase Spindle Positioning

(A) Heat map of genetic interactions between genes with roles in S and M phase spindle positioning (reclustered from (Costanzo et al., 2010)). Interactions are color coded by strength and correspond to epsilon values. Gene names are color coded by function. *YDR149C* is a dubious ORF overlapping the *NUM1* gene.

(B) Yeast spot assays of double mutants between *SCS2* and genes in the M phase cluster. Genes are color coded as in (A).

(C) Wild-type (WT) and *Δscs2* mutant yeast expressing endogenous Tub1 tagged with GFP synchronized in S phase with hydroxyurea. b, bud; m, mother.

(D) Quantification of spindle position in S phase-synchronized wild-type (WT) and *Δscs2* cells by imaging GFP-Tub1 (number of cells counted in each case is given on graph).

(E) As in (D), quantification of spindle position in S phase-synchronized *Δscs2* cells expressing Scs2 and the indicated mutants on plasmids.

(F) As in (D), quantification of spindle position in wild-type and the shs1-cte mutant.

(G and H) Growth assays of the indicated yeast strains on solid (G) or in liquid (H) media (n = 6). All scale bars represent 2 μm. All error bars represent SEM. See also Figure S6.

phenylalanines, resembling a FFAT motif, suggesting this region might interact directly with Scs2 (Figure 7B). Purified recombinant MBP-Scs2ΔTM specifically bound the Num1 FFAT motif tagged with GST (Figure 7C) and by PCA (Figure S6D). Deletion of the Num1 FFAT motif prevented this interaction (Figure S6E) as did the T42A mutation in Scs2 (Figure S6F). The S31A-D32A mutation did not disrupt binding to Num1 (Figure S6G).

Now, we investigated whether the Scs2-Num1 interaction was required for S phase spindle positioning. Deleting the Num1 FFAT motif resulted in twice as many cells with the spindle positioned in the neck, suggesting loss of Scs2 binding affected spindle positioning (Figure 7D). However, this mutant did not appear to misposition the spindle into the bud, suggesting that FFAT motif deletion interfered also with the nuclear migration function of Num1. Incidentally, the FFAT motif is adjacent to the Num1

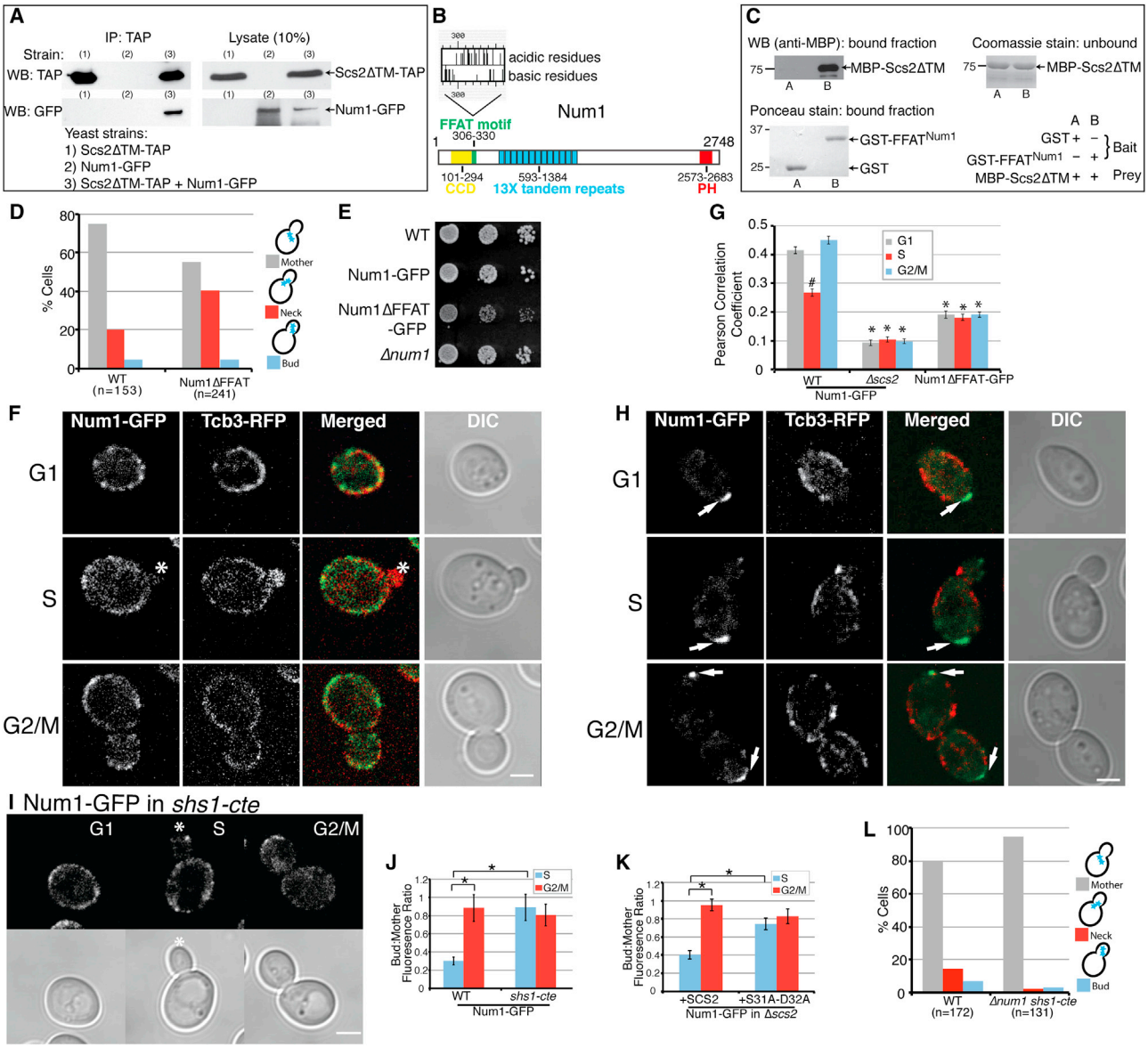

Figure 7. The ER Diffusion Barrier Controls Spindle Positioning through Num1

(A) Cell lysates from yeast expressing the indicated TAP- and GFP-fusion proteins were incubated with IgG beads and the bound fractions (IP) and cell lysates were analyzed by western blotting (WB).

(B) Domain organization of Num1 (from UniProt). Window shows acid/base composition of FFAT motif region (scale, 10 amino acids). FFAT, two phenylalanines in an acidic tract; PH, pleckstrin homology domain; CCD, coiled-coil domain.

(C) In vitro binding of purified recombinant Scs2ΔTM to the FFAT motif of Num1, as performed in Figure 3G.

(D) Quantification of spindle position in S phase-synchronized wild-type (WT) and Num1ΔFFAT cells by imaging GFP-Tub1.

(E) Yeast spot assays of the indicated strains grown on synthetic complete medium.

(F and H) Yeast coexpressing Num1-GFP and Tcb3-RFP in wild-type (F) and the *Δscs2* (H) mutant. Asterisks indicate absence of Num1-GFP localization at the bud cortex. Arrows indicate altered Num1-GFP localizations in the mutant.

(G) Pearson correlation coefficients were calculated for wild-type and *Δscs2* cells expressing Num1-GFP and Tcb3-RFP and for cells expressing Num1ΔFFAT-GFP and Tcb3-RFP. A minimum of 45 cells were analyzed per condition. *$p < 0.0002$ versus WT. #$p < 10^{-12}$ versus WT G1.

(I) Num1-GFP localization in *shs1-cte* cells. The asterisk indicates the appearance of Num1 in the bud cortex.

(J) Quantification of the bud to mother fluorescence ratio of Num1-GFP in wild-type (WT) and the *shs1-cte* mutant. A minimum of 30 cells per category was measured. *$p < 0.0002$.

(K) Similar to (J), but for Num1-GFP in *Δscs2* cells expressing Scs2 and the S31A-D32A mutant from plasmids. *$p < 0.0003$.

(L) Quantification of spindle position in S phase-synchronized wild-type (WT) and *Δnum1 shs1-cte* cells by imaging GFP-Tub1. All scale bars represent 2 μm. All error bars represent SEM.

See also Figures S6 and S7.

CCD, which is required for patch assembly and nuclear migration (Figure 7B) (Tang et al., 2012). We found that the Num1ΔFFAT mutant had a similar frequency of binucleate mothers as deletion of *NUM1* (Figure S7A), indicating that the nuclear migration function was compromised in the Num1ΔFFAT mutant. This was not a result of loss of Scs2 binding, because *Δscs2* cells were not binucleate (Figure S7A). Consistent with both a defect in S phase spindle positioning and M phase nuclear migration, the Num1ΔFFAT mutant had a slow growth phenotype whereas deletion of *NUM1* did not (Figure 7E). Thus, this mutant duplicated the slow growth observed for double mutants of *Δscs2* and *shs1-cte* with M phase components (Figures 6B and 6G).

Scs2 Recruits Num1 to pmaER

The cortical localization of Num1-GFP suggested that it might be associated with pmaER, therefore, we colocalized Num1-GFP with Tcb3-RFP. In wild-type cells, Num1-GFP localized nonuniformly to the cortex and was enriched at the tips of M phase buds (Figure 7F) as previously reported (Farkasovsky and Küntzel, 1995). Num1-GFP was also absent from S phase buds as previously observed (Farkasovsky and Küntzel, 1995; Heil-Chapdelaine et al., 2000). Tcb3-RFP localization appeared similar to Num1-GFP suggesting Num1 was indeed associated with pmaER (Figure 7F). Pearson's correlation coefficient revealed very good correlation between these proteins in G1 and G2/M phases (Figure 7G). In S phase, this correlation decreased ~40% consistent with the absence of Num1-GFP in S phase buds. In *Δscs2* cells, Num1-GFP was no longer distributed along the cortex, but was concentrated in foci at the distal pole of mothers and unbudded cells and at the tips of small and large buds (Figure 7H). These regions did not appear to contain pmaER and corresponded to dynein/dynactin patches (Tang et al., 2012). Consistently, Pearson's correlation coefficient revealed only a very low correlation between Num1-GFP and Tcb3-RFP in *Δscs2* cells (Figure 7G).

Now, we examined the localization of Num1 upon deletion of its FFAT motif; and using mutants of Scs2. FFAT motif deletion dramatically reduced colocalization with Tcb3-RFP and resulted in Num1-GFP having a more punctate localization, suggesting it was no longer associated with pmaER (Figures 7G and S7B). The T42A Scs2 mutant failed to restore cortical localization of Num1-GFP in *Δscs2* cells supporting that Scs2 interacted with the FFAT motif of Num1 (Figures S7C, S7D, and S7F). The S31A-D32A mutant restored Num1-GFP to the cortex indicating Scs2-Shs1 binding was not required to localize Num1 to pmaER (Figures S7E and S7F). To confirm that Num1 was stably associated with the ER we used photobleaching of Num1-GFP and subcellular fractionation. Photobleaching revealed that cortical Num1-GFP had a small mobile fraction of ~15%, which recovered rapidly after bleaching, indicating that ER-associated Num1 did not readily exchange with a cytoplasmic pool (Figures S7G and S7H). Subcellular fractionation of Num1-GFP indicated it co-fractionated with the translocon subunit Sec61, but not a soluble cytoplasmic enzyme (Figure S7I).

The ER Diffusion Barrier Controls the Distribution and Function of Num1 during S Phase

We now tested if the ER diffusion barrier was responsible for restricting Num1 to the mother pmaER during S phase. In both the *shs1-cte* mutant (Figure 7I) and in *Δscs2* cells expressing the S31A-D32A mutant from a plasmid (Figure S7E), Num1-GFP appeared to have diffused into the bud during S phase. Quantification of Num1-GFP in S phase cells revealed that in wild-type the mother to bud ratio approached 3:1, whereas in the *shs1-cte* mutant, this ratio was close to 1:1 (Figure 7J). This was also true for the S31A-D32A mutant expressed in *Δscs2* cells (Figure 7K) indicating that ER-septin tethering restricted Num1-GFP to the mother during S phase. In G2/M phase cells the ratio was close to one, likely a result of expression of Num1 in G2/M phase (Farkasovsky and Küntzel, 1995).

Now, we tested if Num1 was responsible for mispositioning the spindle in cells with a disrupted ER diffusion barrier. We deleted *NUM1* in the *shs1-cte* mutant and found that the spindle no longer mispositioned into the bud and neck as it did in the *shs1-cte* single mutant and instead was positioned entirely within the mother (Figure 7L; compare to Figure 6F). Interestingly, this phenotype also indicated that the ER diffusion barrier did not function to restrict the passive diffusion of the spindle between mother and bud. Thus, the ER diffusion barrier retained Num1 in the mother, which prevented it from pulling the spindle into the bud during S phase.

DISCUSSION

How might ER-septin tethering create the ER diffusion barrier? Perhaps the Scs2-Shs1 tether positions ER tubules traversing the neck in close proximity to septin filaments such that ER proteins with domains on the cytosolic face of the ER are sterically hindered within the neck. Continuous septin structures are found in close contact with the PM, usually within a distance of 10 nm (Faty et al., 2002), and this is sufficient to restrict the diffusion of PM proteins. Therefore, close proximity of ER to septins might produce a similar effect, restricting the diffusion of ER proteins between mother and bud. Lumenal proteins appear to be free from the barrier (Luedeke et al., 2005). This suggests the barrier exists only on the cytoplasmic leaflet of the ER membrane. Because Scs2 is a tail-anchored ER protein with no lumenal domain, a proximity-based Scs2-Shs1 tethering mechanism would likely be ineffective in restricting diffusion of lumenal proteins.

Another possibility is that Shs1 might impose ordering of Scs2 on the ER at the bud neck, creating a net on the cytosolic face of the ER membrane to catch diffusing ER proteins. The MSP domain of Scs2 is highly homologous to MSP proteins in nematodes, which lack transmembrane domains, but which form membrane-associated cytoskeletal "mesh"-like structures that are responsible for sperm motility (Sepsenwol et al., 1989). The structure of the Scs2 MSP domain shares an identical fold with nematode MSP (Kaiser et al., 2005), suggesting that Scs2 has the capacity to form related mesh-like structures on the ER. However, the MSP domain dimer interface is not perfectly conserved in Scs2, suggesting perhaps that interaction with Shs1 facilitates Scs2 oligomerization and mesh formation at the bud neck to create the ER diffusion barrier.

Restricting diffusion of ER proteins along ER tubules that traverse the bud neck presents a unique problem, because most ER proteins will likely be distributed around the circumference of the tubules. If ER-septin tethering establishes the

ER diffusion barrier by proximity to septins, then septins would need to surround ER tubules. Recent work reconstituting septin interactions in vitro shows that in addition to forming straight filaments, septins form filamentous rings and gauze-like structures (Garcia et al., 2011). The rings have diameters in the range of 400–850 nm, which are similar in size to the yeast bud neck. Remarkably, gauze-like structures form within the rings that have ~30 nm holes with regular spacing, resembling a waffle. Given that the diameters of ER tubules are in the range of 20–50 nm, ER tubules could foreseeably pass through the holes in the gauze, enabling septins to surround the tubules. Interaction of Scs2 with the CTE of Shs1 within the holes in the gauze could therefore establish a proximity-based ER diffusion barrier that surrounds ER tubules.

ER-septin tethering maintains the ER diffusion barrier throughout the cell cycle, including within the nuclear ER during mitosis as the nucleus is pulled through the bud neck. The diameter of the nucleus is much larger than an ER tubule and would require that the Scs2-Shs1 tether and perhaps the septin gauze be remodeled during nuclear migration. Phosphorylation of the Shs1 CTE promotes gauze formation in vitro (Garcia et al., 2011) and CTE phosphorylation in vivo is cell-cycle-dependent and dramatically decreases in M phase (Egelhofer et al., 2008). This suggests that dephosphorylation of Shs1 in preparation for mitosis could remodel the septin gauze and the Shs1-Scs2 tether, enabling the nuclear ER and spindle to be pulled through the bud neck, while maintaining the ER diffusion barrier.

ER-septin tethering likely creates ER diffusion barriers in other polarized cell types. In dendritic spines and dendritic branch points of neurons there is restricted diffusion of ER proteins (Cui-Wang et al., 2012). Septins localize to the spine base and at branch points (Tada et al., 2007), suggesting that ER-septin tethering could polarize the ER in dendrites. Polarization of the IP3 receptor in dendritic spines of mouse Purkinje cells is required for mGluR-dependent calcium signaling, and mutations that prevent its polarization cause severe ataxia in mice that mimics amyotrophic lateral sclerosis (ALS) (Wagner et al., 2011). This implies an important role for ER diffusion barriers in nerve transmission. Mutations in the MSP domain of VAP-B, the human homolog of Scs2, cause ALS (Nishimura et al., 2004), indicating perhaps that defective ER-septin tethering in dendrites is a contributing factor in ALS. Septins have also now been found to play a role in regulating calcium traffic at PM-ER junctions (Sharma et al., 2013), suggesting that diffusion barriers created by VAP-septin tethering may be important at these and other ER junctions. Last, septins are found at the base of many ER-containing polarized structures including filopodia, pseudopodia, cilia, and the cytokinetic cleavage furrow, and VAP proteins localize throughout the ER in most cell types implying that ER-septin tethering may be of widespread importance in biology.

EXPERIMENTAL PROCEDURES

Yeast Strains, Growth Conditions, and Manipulations

All yeast were grown at 30°C with shaking in synthetic defined (SD) media with the appropriate dropouts and 2% dextrose unless otherwise stated. All fusion proteins were generated by tagging the endogenous gene in haploid yeast unless otherwise stated. For plasmids, yeast strains, additional growth conditions, mutagenesis, and manipulations, see Supplemental Information.

Affinity Purification and Mass Spectrometry

Scs2ΔTM and Epo1 were TAP-tagged and purified from yeast lysates by one-step purification with IgG beads. For Scs2ΔTM, SILAC methodology was employed, whereas for Epo1, a control purification using an untagged control strain was used for comparison. Copurifying proteins were identified by LC/MS/MS using a linear-trapping quadrupole-Orbitrap mass spectrometer (LTQ-Orbitrap Velos; ThermoFisher Scientific) on-line coupled to an Agilent 1200 Series HPLC using a nanospray ionization source (ThermoFisher Scientific). See Supplemental Information for further details.

Protein Subcellular Localization by Confocal Microscopy

Log phase live yeast cells were imaged using a Zeiss LSM-5 Pascal confocal microscope. ImageJ software (NIH) was used for all quantifications of protein subcellular localization and a minimum of 25 cells were measured per condition. See Supplemental Information for further details.

Photobleaching Experiments

Photobleaching was performed on live log phase yeast using an Olympus FV1000 confocal microscope controlled by the Olympus Fluoview Version 3.0 Software. For all diffusion barrier photobleaching experiments, three unbleached regions of interest (ROIs) in the peripheral ER were monitored in the mother of each bleached cell. Normalized fluorescence data were analyzed using one phase association nonlinear regression analysis using Prism software (GraphPad). See Supplemental Information for further details.

Genetic Interactions

Synthetic genetic array (SGA) analysis was performed by mating a *Δscs2::URA3* query strain to the nonessential yeast deletion collection arrayed at 1536 density using a Singer RoToR Colony Arraying robot and selecting for single- and double-mutant arrays through a series of replica pinning steps. Balony software was used to measure spot sizes, determine cut-off values for genetic interactions and define double-mutant strains that showed statistically significant alterations in growth. See Supplemental Information for further details.

In Vitro Binding and Coimmunopurification Experiments

For in vitro binding, MBP and GST fusion proteins were expressed and purified from *Escherichia coli*. Binding experiments were performed by incubating purified MBP fusions with GST fusions bound to glutathione beads. For coimmunopurifications, cell lysates from log phase yeast were incubated with IgG beads overnight at 4°C. See Supplemental Information for further details. See also the Extended Experimental Procedures.

SUPPLEMENTAL INFORMATION

Supplemental Information includes Extended Experimental Procedures, seven figures, and five tables and can be found with this article online at http://dx.doi.org/10.1016/j.cell.2014.06.033.

ACKNOWLEDGMENTS

This research was supported by grants from the Canadian Institute of Health Research (CIHR), the Michael Smith Foundation for Health Research (MSFHR), and the Canada Foundation for Innovation (CFI). C.J.R.L. and T.M. are CIHR New Investigators and MSFHR Scholars, C.J.R.L. is a Tula Foundation Investigator, and L.J.F. is the Canada Research Chair in Organelle Proteomics.

Received: February 6, 2014
Revised: May 16, 2014
Accepted: June 19, 2014
Published: July 31, 2014

REFERENCES

Caudron, F., and Barral, Y. (2009). Septins and the lateral compartmentalization of eukaryotic membranes. Dev. Cell *16*, 493–506.

Chao, J.T., Foster, L.J., and Loewen, C.J. (2009). Identification of protein complexes with quantitative proteomics in S. cerevisiae. J. Vis. Exp. *25*, pii: 1225.

Costanzo, M., Baryshnikova, A., Bellay, J., Kim, Y., Spear, E.D., Sevier, C.S., Ding, H., Koh, J.L., Toufighi, K., Mostafavi, S., et al. (2010). The genetic landscape of a cell. Science *327*, 425–431.

Cui-Wang, T., Hanus, C., Cui, T., Helton, T., Bourne, J., Watson, D., Harris, K.M., and Ehlers, M.D. (2012). Local zones of endoplasmic reticulum complexity confine cargo in neuronal dendrites. Cell *148*, 309–321.

Dobbelaere, J., and Barral, Y. (2004). Spatial coordination of cytokinetic events by compartmentalization of the cell cortex. Science *305*, 393–396.

Egelhofer, T.A., Villén, J., McCusker, D., Gygi, S.P., and Kellogg, D.R. (2008). The septins function in G1 pathways that influence the pattern of cell growth in budding yeast. PLoS ONE *3*, e2022.

Evangelista, M., Blundell, K., Longtine, M.S., Chow, C.J., Adames, N., Pringle, J.R., Peter, M., and Boone, C. (1997). Bni1p, a yeast formin linking cdc42p and the actin cytoskeleton during polarized morphogenesis. Science *276*, 118–122.

Farkasovsky, M., and Küntzel, H. (1995). Yeast Num1p associates with the mother cell cortex during S/G2 phase and affects microtubular functions. J. Cell Biol. *131*, 1003–1014.

Faty, M., Fink, M., and Barral, Y. (2002). Septins: a ring to part mother and daughter. Curr. Genet. *41*, 123–131.

Fischer, M.A., Temmerman, K., Ercan, E., Nickel, W., and Seedorf, M. (2009). Binding of plasma membrane lipids recruits the yeast integral membrane protein Ist2 to the cortical ER. Traffic *10*, 1084–1097.

Furuita, K., Jee, J., Fukada, H., Mishima, M., and Kojima, C. (2010). Electrostatic interaction between oxysterol-binding protein and VAMP-associated protein A revealed by NMR and mutagenesis studies. J. Biol. Chem. *285*, 12961–12970.

Garcia, G., 3rd, Bertin, A., Li, Z., Song, Y., McMurray, M.A., Thorner, J., and Nogales, E. (2011). Subunit-dependent modulation of septin assembly: budding yeast septin Shs1 promotes ring and gauze formation. J. Cell Biol. *195*, 993–1004.

Heil-Chapdelaine, R.A., Oberle, J.R., and Cooper, J.A. (2000). The cortical protein Num1p is essential for dynein-dependent interactions of microtubules with the cortex. J. Cell Biol. *151*, 1337–1344.

Iwase, M., Luo, J., Bi, E., and Toh-e, A. (2007). Shs1 plays separable roles in septin organization and cytokinesis in Saccharomyces cerevisiae. Genetics *177*, 215–229.

Kaiser, S.E., Brickner, J.H., Reilein, A.R., Fenn, T.D., Walter, P., and Brunger, A.T. (2005). Structural basis of FFAT motif-mediated ER targeting. Structure *13*, 1035–1045.

Loewen, C.J., Roy, A., and Levine, T.P. (2003). A conserved ER targeting motif in three families of lipid binding proteins and in Opi1p binds VAP. EMBO J. *22*, 2025–2035.

Loewen, C.J., Young, B.P., Tavassoli, S., and Levine, T.P. (2007). Inheritance of cortical ER in yeast is required for normal septin organization. J. Cell Biol. *179*, 467–483.

Luedeke, C., Frei, S.B., Sbalzarini, I., Schwarz, H., Spang, A., and Barral, Y. (2005). Septin-dependent compartmentalization of the endoplasmic reticulum during yeast polarized growth. J. Cell Biol. *169*, 897–908.

Michnick, S.W., Ear, P.H., Manderson, E.N., Remy, I., and Stefan, E. (2007). Universal strategies in research and drug discovery based on protein-fragment complementation assays. Nat. Rev. Drug Discov. *6*, 569–582.

Newman, J.R., Wolf, E., and Kim, P.S. (2000). A computationally directed screen identifying interacting coiled coils from Saccharomyces cerevisiae. Proc. Natl. Acad. Sci. USA *97*, 13203–13208.

Nishimura, A.L., Mitne-Neto, M., Silva, H.C., Richieri-Costa, A., Middleton, S., Cascio, D., Kok, F., Oliveira, J.R., Gillingwater, T., Webb, J., et al. (2004). A mutation in the vesicle-trafficking protein VAPB causes late-onset spinal muscular atrophy and amyotrophic lateral sclerosis. Am. J. Hum. Genet. *75*, 822–831.

Pruyne, D., Legesse-Miller, A., Gao, L., Dong, Y., and Bretscher, A. (2004). Mechanisms of polarized growth and organelle segregation in yeast. Annu. Rev. Cell Dev. Biol. *20*, 559–591.

Sepsenwol, S., Ris, H., and Roberts, T.M. (1989). A unique cytoskeleton associated with crawling in the amoeboid sperm of the nematode, Ascaris suum. J. Cell Biol. *108*, 55–66.

Sharma, S., Quintana, A., Findlay, G.M., Mettlen, M., Baust, B., Jain, M., Nilsson, R., Rao, A., and Hogan, P.G. (2013). An siRNA screen for NFAT activation identifies septins as coordinators of store-operated Ca2+ entry. Nature *499*, 238–242.

Shcheprova, Z., Baldi, S., Frei, S.B., Gonnet, G., and Barral, Y. (2008). A mechanism for asymmetric segregation of age during yeast budding. Nature *454*, 728–734.

Shepard, K.A., Gerber, A.P., Jambhekar, A., Takizawa, P.A., Brown, P.O., Herschlag, D., DeRisi, J.L., and Vale, R.D. (2003). Widespread cytoplasmic mRNA transport in yeast: identification of 22 bud-localized transcripts using DNA microarray analysis. Proc. Natl. Acad. Sci. USA *100*, 11429–11434.

Spira, F., Mueller, N.S., Beck, G., von Olshausen, P., Beig, J., and Wedlich-Söldner, R. (2012). Patchwork organization of the yeast plasma membrane into numerous coexisting domains. Nat. Cell Biol. *14*, 640–648.

Tada, T., Simonetta, A., Batterton, M., Kinoshita, M., Edbauer, D., and Sheng, M. (2007). Role of Septin cytoskeleton in spine morphogenesis and dendrite development in neurons. Curr. Biol. *17*, 1752–1758.

Takizawa, P.A., DeRisi, J.L., Wilhelm, J.E., and Vale, R.D. (2000). Plasma membrane compartmentalization in yeast by messenger RNA transport and a septin diffusion barrier. Science *290*, 341–344.

Tang, X., Germain, B.S., and Lee, W.-L. (2012). A novel patch assembly domain in Num1 mediates dynein anchoring at the cortex during spindle positioning. J. Cell Biol. *196*, 743–756.

Tarassov, K., Messier, V., Landry, C.R., Radinovic, S., Serna Molina, M.M., Shames, I., Malitskaya, Y., Vogel, J., Bussey, H., and Michnick, S.W. (2008). An in vivo map of the yeast protein interactome. Science *320*, 1465–1470.

Tong, A.H., Lesage, G., Bader, G.D., Ding, H., Xu, H., Xin, X., Young, J., Berriz, G.F., Brost, R.L., Chang, M., et al. (2004). Global mapping of the yeast genetic interaction network. Science *303*, 808–813.

Toulmay, A., and Prinz, W.A. (2012). A conserved membrane-binding domain targets proteins to organelle contact sites. J. Cell Sci. *125*, 49–58.

Versele, M., Gullbrand, B., Shulewitz, M.J., Cid, V.J., Bahmanyar, S., Chen, R.E., Barth, P., Alber, T., and Thorner, J. (2004). Protein-protein interactions governing septin heteropentamer assembly and septin filament organization in Saccharomyces cerevisiae. Mol. Biol. Cell *15*, 4568–4583.

Wagner, W., Brenowitz, S.D., and Hammer, J.A., 3rd. (2011). Myosin-Va transports the endoplasmic reticulum into the dendritic spines of Purkinje neurons. Nat. Cell Biol. *13*, 40–48.

Yeh, E., Skibbens, R.V., Cheng, J.W., Salmon, E.D., and Bloom, K. (1995). Spindle dynamics and cell cycle regulation of dynein in the budding yeast, Saccharomyces cerevisiae. J. Cell Biol. *130*, 687–700.